Digestive and Liver Disease 58 (2026) 390–396

Contents lists available at ScienceDirect

Digestive and Liver Disease

journal homepage: www.elsevier.com/locate/dld

Oncology

Nuclear miR-3920 expression in hepatocellular carcinoma is associated with stemness marker expression and poorer prognosis

Hyunjin Park[a,b,1], Seunghye Kim[a,1], Hyejung Lee[a], Hee Young Na[a,c], Jeong Eun Yoo[d], Haeryoung Kim[a,e,*]

[a] Department of Pathology, Seoul National University College of Medicine, Seoul, 03080, Republic of Korea
[b] Department of Pathology, Gangnam Severance Hospital, Yonsei University College of Medicine, Seoul, 06273, Republic of Korea
[c] Department of Pathology, Seoul National University Bundang Hospital, Seoul National University College of Medicine, Seongnam, 13605, Republic of Korea
[d] Department of Pathology, Yonsei University College of Medicine, Seoul, 03722, Republic of Korea
[e] Department of Pathology, Seoul National University Hospital, Seoul National University College of Medicine, Seoul, 03080, Republic of Korea.

ARTICLE INFO

Article history:
Received 4 October 2024
Accepted 25 December 2025
Available online 16 January 2026

Keywords:
Hepatocellular carcinoma
Stemness
MicroRNA
miR-3920

ABSTRACT

Background: Stemness-related marker expression in hepatocellular carcinomas (HCC) has been associated with aggressive behavior. The association between miRNA expression and HCC stemness remains unclear.
Aims: To identify miRNAs associated with stemness marker expression in HCC and their clinical significance.
Methods: MicroRNA microarray analysis was performed to identify microRNAs that were differentially expressed between EpCAM-positive and EpCAM-negative HCCs. The subcellular localization and expression level of miR-3920 was evaluated by locked nucleic acid-in situ hybridization analysis on surgically resected HCCs and paired non-tumor liver (NT).
Results: There was significant upregulation of miR-3920 in EpCAM-positive HCCs compared to EpCAM-negative cases ($p = 0.025$). Nuclear miR-3920 expression ($p < 0.001$) and the nuclear-to-total miR-3920 signal ratio ($p < 0.001$) were significantly higher in HCCs compared with NT. High nuclear-to-total miR-3920 signal ratio was positively correlated with stemness marker expression (EpCAM, $p = 0.002$; K19, $p < 0.001$), the presence of microvascular invasion ($p = 0.004$), major vessel invasion ($p = 0.001$) and mitosis ($p < 0.001$). Higher nuclear-to-total miR-3920 signal ratio was associated with significantly decreased overall survival ($p = 0.010$) and disease-free survival ($p = 0.016$).
Conclusion: Increased expression of miR-3920 in the nuclei of HCC tumor cells was associated with stemness-related marker expression and aggressive clinicopathological features of HCC, suggesting a possible role for miR-3920 in HCC stemness and progression.

1. Introduction

Despite recent developments in treatment, hepatocellular carcinoma (HCC) is currently the sixth most common cause of cancer-related death, with a 5-year overall survival (OS) rate of less than 20%. [1–3] HCC is a heterogeneous neoplasm, in both morphology and morphological profile, and several morphomolecular subtypes of HCC have been proposed over the past several years [4,5]. HCC expressing markers associated with “stemness”, such as epithelial cell adhesion molecule (EpCAM), keratin 19 (K19) and SALL4, is one of the proposed subtypes and is defined as an HCC that is compatible with a diagnosis of HCC morphologically but express these markers [5,6]. This subgroup of HCCs has received increasing attention during the past decades, as these tumors have been associated with aggressive biological behavior, decreased patient survival, and resistance to locoregional and systemic treatment [6].

At least 60% of human genes are estimated to be regulated by microRNAs (miRNAs), and miRNAs may have oncogenic or tumor suppressive roles in tumorigenesis [7]. Although there are numerous studies demonstrating the miRNA expression profiles in HCCs [8–12], only a few studies have examined the miRNA profiles of HCCs expressing stemness-related markers. Guo et al. demon-

* Corresponding author at: Department of Pathology, Seoul National University Hospital, Seoul National University College of Medicine, Basic Science Building #101, 103 Daehak-ro, Jongno-gu, Seoul 03080, Korea.
E-mail address: haeryoung.kim@snu.ac.kr (H. Kim).
[1] Contributed equally as co-first authors.

https://doi.org/10.1016/j.dld.2025.12.023

strated that miR-448 inhibits stemness maintenance in HCCs by controlling the AMP-activated protein kinase signaling pathway [13]. Another study demonstrated a role for miR-497 in suppressing stemness properties of HCC by directly targeting SALL4 [14]. Upregulation of several miRNAs, including the miR-181 family, miR-155, and miR-200b miRNA expression, have been demonstrated in EpCAM-positive HCCs by miRNA expression profiling studies [15]. However, as miRNA expression profiling is performed on total RNA obtained from bulk tissue, it is not possible to identify the source of the elevated miRNAs at the subcellular level. In this study, we performed miRNA expression profiling following by locked nucleic acid fluorescent in-situ hybridization (LNA-FISH). We identified miR-3920 to be differentially expressed in EpCAM-positive HCCs, and that increased nuclear miR-3920 transcripts was associated with EpCAM and K19 expression, clinicopathological features associated with aggressive behavior and poor survival.

2. Methods

2.1. miRNA microarray

Formalin-fixed paraffin-embedded (FFPE) tissue from 9 cases of HCCs that were surgically resected at Seoul National University Bundang Hospital, from 2011 to 2012, were selected for miRNA microarray screening. This study was approved by the Institutional Review Board of Seoul National University Bundang Hospital (B-2406-904-303). This microarray cohort comprised 4 EpCAM-positive and 5 EpCAM-negative cases; the cohort was balanced according to EpCAM expression status. Ten unstained sections of 10μm-thickness were obtained from each of the FFPE tissue blocks and the tumor components were carefully macrodissected by a pathologist (HK). Total RNA extraction was performed using Qiagen miRNeasy FFPE Kit (Qiagen, Valencia, CA, USA), according to the manufacturer's instructions, and the extracted total RNA was evaluated using NanoDrop spectrophotometer (ND-1000). Hybridization was performed on the total RNA samples labeled with alkaline phosphatase, using 7th generation miRCURY LNA^{TM} microRNA Array (Exiqon, Vedbaek, Denmark), according to the manufacturer's instructions. Signal data and images were scanned by Agilent C scanner and scanned images were analyzed with Feature Extraction v10.7.3.1 software. The quantile normalization was used for the analysis of DNA chip results using signal intensity data. Differentially expressed genes according to EpCAM expression status were identified using GeneSpring GX 13.0 software, and a $\geq$1.5 fold change in miRNA expression was interpreted as significant.

2.2. Tissue microarray construction

Tissue microarrays were constructed from 275 consecutive cases of HCC that were surgically resected at Seoul National University Bundang Hospital between 2003 and 2013. The tissue microarrays consisted of 2mm-diameter cores from HCCs and matched non-neoplastic liver tissues (NT), and one to three cores were sampled from HCCs depending on the amount of histological heterogeneity present. The clinicopathological information was obtained by reviewing electronic medical records, including patient age at the time of diagnosis, sex, etiology, preoperative serum alpha-fetoprotein (AFP) level, tumor size, multiplicity, histologic grade, vascular invasion status, and mitotic index. Multiplicity included intrahepatic metastases and multiple occurrences. Major vascular invasion was defined as invasion of the main portal vein, or the right, middle and left hepatic veins. OS was defined as the interval between surgical intervention to the date of death due to HCC, and disease-free survival (DFS) as the interval from surgical intervention to local or distant recurrence.

2.3. Immunohistochemistry and LNA-FISH

Four μm-thick sections were obtained from the tissue microarray blocks and subjected to immunohistochemical staining for EpCAM (mouse monoclonal, VU-1D9, 1:1,500, Millipore, Temecula, United States), K19 (mouse monoclonal, BA17, 1:200, Dako, Glostrup, Denmark), and Ki-67 (mouse monoclonal, MIB-1, 1:100, Dako, Glostrup, Denmark) using the Ventana BenchMark GX automated platform (Ventana Medical Systems). Membranous and/or cytoplasmic staining in $\geq$5% of the tumor cells were counted as positive for EpCAM and K19. Ki-67 labeling indices were assessed at 400x magnification from the hotspots of each core, as the number of Ki-67-labeled tumor cell nuclei/total number of tumor cell nuclei x 100%.

LNA-FISH was performed on 4μm-thick sections obtained from the tissue microarray blocks, as previously described [16]. Briefly, unstained sections were deparaffinized and rehydrated sequentially with graded ethanol. Prehybridization was performed for 20 min at room temperature, followed by hybridization with the hsa-miR-3920 probe (miRCURY LNA^{TM} microRNA Detection probe, Exiqon, Vedbaek, Denmark). Tissue sections were the incubated with blocking buffer, followed by FITC/HRP solution, tyramide amplification solution, and DAPI staining solution. The LNA-FISH slides were observed under a fluorescent microscope (BX51, Olympus Optical, Tokyo, Japan) at 1,000x magnification, and the numbers of fluorescent signals (spots) were assessed using the QuPath software (https://qupath.github.io/). Two 1,000x fields with the highest number of signals were selected after screening each 2 mm tissue microarray core, and images were captured using a digital microscope camera (DP70, Olympus Optical, Tokyo, Japan). The signals in the nuclei and cytoplasm were counted separately for each cell, yielding nuclear counts, cytoplasmic counts, and total counts (sum of nuclear and cytoplasmic counts). The average counts/cell were calculated for each case.

2.4. Cell lines and culture

Four human hepatocellular carcinoma (HCC) cell lines, SNU423, SNU475, Hep3B, and Huh7 were obtained from the Korean Cell Line Bank (Seoul, Korea) and cultured in DMEM (Biowest, Nuaillé, France) with 10% heat-inactivated FBS (Biowest) and penicillin/streptomycin (100 U/mL penicillin, 100 µg/mL streptomycin; Gibco, Grand Island, NY, USA) at 37°C in 5% CO_2.

2.5. Real-time quantitative PCR (RT-qPCR)

miRNA isolation was performed using the mirVana^{TM} miRNA Isolation Kit with phenol (Invitrogen^{TM}, Carlsbad, CA, USA) according to the manufacturer's instructions. The transcription into cDNA was synthesized using the TaqMan^{TM} Advanced miRNA cDNA Synthesis Kit (Applied Biosystems^{TM}, Foster City, CA, USA) and qPCR was performed using TaqMan^{TM} Universal PCR Master Mix (Applied Biosystems^{TM}) and TaqMan^{TM} Advanced miRNA assay (Applied Biosystems^{TM}) for hsa-miR-3920 (Assay ID: 479741_mir; mature miRNA sequence: 5'-ACUGAUUAUCUUAACUCUCUGA-3'). PCR reactions were performed using a QuantStudio^{TM} 3 Real-Time PCR System (Applied Biosystems^{TM}) at 50°C for 2 minutes and 95°C for 15 seconds, followed by 40 cycles of 15 seconds at 95°C and 1 minute at 60°C. As an endogenous control, hsa-miR-16-5p (Assay ID: 477860_mir; mature miRNA sequence: 5'-UAGCAGCACGUAAAUAUUGGCG-3') was used for normalization. Each reaction was performed in triplicate. A non-template control was included in all experiments as a negative control. Relative miR-3920 expression levels were calculated using the comparative Ct (2-$\Delta\Delta$Ct) method.

2.6. Transfection and western blot

Cells were transfected using Lipofectamine™ RNAiMAX Transfection Reagent (Invitrogen™) according to the manufacturer's instructions. Hep3B and Huh7 cells (at 50-60% confluency) were transfected with 20 uM and 40 uM of target miRNA, respectively. Target miRNAs were as follows: AccuTarget miRNA Negative Control, mimic #1 (Bioneer, Daejeon, Korea) and AccuTarget Human miR-3920 Mimic (Bioneer). At 72 hours post-transfection, cell lysates were prepared from RIPA Lysis and Extraction buffer (Thermo Scientific™, Waltham, MA, USA) containing a mixture of protease and phosphatase inhibitors. After separation by SDS-PAGE (Bolt™ Bis-Tris Plus Mini Protein Gels 8%, 1.0 mm, WedgeWell™ format 10-well (Invitrogen™)), proteins were transferred to a PVDF membrane via the iBlot™ 2 Dry Blotting System. The membrane was then incubated in blocking buffer made of 5% (w/v) nonfat dried milk, 0.01% (v/v) Tween 20 in Tris-buffered saline (TBST) at RT for 45 minutes. Subsequently, the membranes were incubated with primary antibody anti-EpCAM (VU-1D9, Sigma-Aldrich, St. Louis, MO, USA) or anti-vinculin (7F9, Santa Cruz Biotechnology, Dallas, TX, USA) diluted in TBST (1:1,000, v/v) at 4°C overnight, followed by HRP-conjugated secondary antibodies (Goat Anti-Mouse IgG H&L, 1:1,000, Abcam, Cambridge, UK). The protein bands were visualized using SuperSignal™ West Pico PLUS Chemiluminescent Substrate (Thermo Scientific™) and an Amersham Imager 680 (GE Healthcare Life Sciences, Chicago, IL, USA) and quantified using National Institutes of Health (NIH) ImageJ software. Vinculin was used as a normalization control.

2.7. Statistical analysis

All statistical analyses were conducted using IBM SPSS Statistics version 19 (IBM Corp., Armonk, NY, USA). Chi-square and t-tests were performed as deemed appropriate. Univariate analyses for OS and DFS were performed using the Cox proportional hazards model regression analysis, Kaplan–Meier method and log-rank tests. Statistical significance was defined as $p < 0.05$. Statistically significant variables from the univariate analysis and those that met the proportional hazard assumptions were further analyzed by the Cox proportional hazard method.

3. Results

3.1. MiR-3920 is differentially expressed in EpCAM-positive HCCs

The clinicopathological characteristics of the miRNA microarray cohort are summarized in Supplementary table 1. The mean age of the patients was 52.4 years (range: 38-72 years), and 77.8% patients were male. All cases had either hepatitis B virus (HBV, 88.9%) or hepatitis C virus (HCV, 11.1%)-related chronic liver disease in the background liver. Analysis for differentially expressed genes according to EpCAM expression status identified 122 upregulated and 30 downregulated miRNAs in EpCAM-positive HCCs compared with EpCAM-negative HCCs. Of these, miR-3920 was significantly upregulated in EpCAM-positive HCCs ($p = 0.025$) (Supplementary Fig. 1).

3.2. In situ analysis for miR-3920 expression in HCCs and non-neoplastic liver tissues

The clinicopathological characteristics of the HCC tissue microarray cohort are summarized in Table 1. A total of 267 cases were finally analyzed, as a result of tissue loss during the LNA-FISH experiment. In summary, the mean age of the patients was 58.5 years, and 76.7% were male. The most common etiology was hepatitis B virus (HBV, 71.3%), followed by hepatitis C virus (8.4%) and alcohol (5.8%). There were 35 (12.7%) cases with non-alcoholic fatty liver disease (NAFLD). The mean size of the HCCs was 4.0 cm and 18.9% were multiple. The majority of HCCs were Edmondson-Steiner grade III (60.0%). Microvascular invasion and major vascular invasion were present in 38.9% and 7.3%, respectively.

On comparison between HCC tumor cells and paired NT, the total miR-3920 signal counts were significantly higher in NT compared with HCC (NT: 63.97 ± 72.43/cell, range: 6.88-1099.47 vs. HCC: 39.79 ± 23.41/cell, range: 9.89-140.59; $p < 0.001$). In addition, the total miR-3920 signal counts were significantly higher in EpCAM-negative cases (positive: 41.03 ± 2.20/cell, negative: 48.72 ± 1.88/cell, $p = 0.014$). However, there were significantly higher numbers of nuclear miR-3920 spots in HCC compared with NT (HCC: 6.43 ± 3.35/cell, range: 1.35-30.50 vs. NT: 4.69 ± 2.84/cell, range: 0.58-17.96; $p < 0.001$), and the ratio of nuclear-to-total miR-3920 signals was higher in HCC (0.155 ± 0.076/cell, range: 0.035-0.559) compared with NT (0.077 ± 0.040/cell, range: 0.006-0.278; $p < 0.001$) (Fig. 1).

Further analysis was performed by grouping the HCCs based on the median nuclear-to-total miR-3920 ratio (0.141), as miR-3920^{hi} (n=134) and miR-3920^{lo} HCCs (n=133). The miR-3920^{hi} HCCs were more frequently associated with EpCAM ($p = 0.002$) and K19 ($p < 0.001$) expression, HBV-related etiology ($p = 0.012$), microvascular invasion ($p = 0.004$), major vessel invasion ($p = 0.001$), and higher mitotic indices ($p < 0.001$), and showed a negative correlation with age at diagnosis ($p < 0.001$) and NAFLD ($p = 0.009$) (Fig. 2).

3.3. Survival analysis

The median follow-up period was 70 months (range, 0 to 166 months). Kaplan-Meier analysis revealed significantly decreased OS for patients with miR-3920^{hi} HCCs ($p = 0.010$), multiple HCCs ($p = 0.007$), HCCs with large tumor size (≥5 cm, $p = 0.020$), microvascular invasion ($p = 0.048$) and major vessel invasion ($p = 0.019$) (Fig. 3A). DFS was significantly lower for patients with miR-3920^{hi} HCCs ($p = 0.016$), multiple HCCs ($p = 0.001$), and HCCs with microvascular invasion ($p = 0.048$) (Fig. 3B).

Table 2 summarizes the analysis results for factors predictive of OS and DFS. Significant predictive factors for OS on multivariable analysis were large (≥5 cm) tumor size [hazard ratio (HR), 2.082; 95% confidence interval (CI), 1.058-4.098; $p = 0.034$], multiplicity (HR, 2.074; 95% CI, 1.021-4.213; $p = 0.044$), and miR-3920^{hi} status (HR, 2.318; 95% CI, 1.167-4.603; $p = 0.016$). MiR-3920^{hi} status was also a significant predictive factor for DFS on multivariable analysis (HR, 1.439; 95% CI, 1.041-1.987; $p = 0.027$), in addition to tumor multiplicity (HR, 1.812; 95% CI, 1.234-2.661; $p = 0.002$).

3.4. EpCAM expression in HCC cell lines with ectopic miR-3920 expression

To investigate whether miR-3920 plays a role in the regulation of EpCAM expression, EpCAM-positive (Hep3B and Huh7) and EpCAM-negative HCC cell lines (SNU423, SNU475) were transfected with miR-3920 mimic. After transfection, there was no evidence of EpCAM expression in SNU423 and SNU475 cells, suggesting that EpCAM is not induced in EpCAM-negative cells by miR-3920 transfection. In the EpCAM-positive Hep3B and Huh7 cells, ectopic miR-3920 expression resulted in a slight decrease in EpCAM expression, although not significant (Supplementary Fig. 2).

4. Discussion

In this study, we demonstrate that miR-3920 was differentially expressed in HCCs expressing stemness-related markers. In addition, high nuclear miR-3920 expression in HCCs was correlated

Table 1
Clinicopathological and immunohistochemical characteristics of hepatocellular carcinomas according to miR-3920 expression status.

Parameters	Number (%)[a]	miR-3920^{hi} (n=134)	miR-3920^{lo} (n=133)	p-value
Age (year)	58.5 ± 11.3	55.8 ± 10.9	60.6 ± 11.2	***<0.001***
Sex				
Male	211 (76.7)	99 (73.9)	104 (78.2)	0.409
Female	64 (23.3)	35 (26.1)	29 (21.8)	
Etiology				0.051
Hepatitis B	196 (71.3)	106 (79.1)	86 (64.7)	
Hepatitis C	23 (8.4)	9 (6.7)	14 (10.5)	
Hepatitis B and C	1 (0.4)	0 (0)	1 (0.8)	
Alcohol	16 (5.8)	6 (4.5)	7 (5.3)	
NAFLD	35 (12.7)	10 (7.5)	24 (18.0)	
Unknown	4 (1.5)	3 (2.2)	1 (0.8)	
Serum AFP (IU/mL)	1359.3 ± 5325.9	1633.5 ± 5300.0	1146.7 ± 5497.0	0.467
Tumor size (cm)[b]	4.0 ± 2.7	4.0 ± 2.7	3.9 ± 2.7	0.855
Multiplicity (present)	52 (18.9)	29 (21.6)	21 (15.8)	0.220
Edmondson-Steiner grade				0.367
I	3 (1.1)	0 (0)	3 (2.3)	
II	75 (27.3)	36 (26.9)	37 (27.8)	
III	165 (60.0)	82 (61.2)	77 (57.9)	
IV	32 (11.6)	16 (11.9)	16 (12.0)	
Microvascular invasion (present)	107 (38.9)	63 (47.0)	40 (30.1)	***0.004***
Major vessel invasion[c] (present)	20 (7.3)	17 (12.7)	3 (2.3)	***0.001***
Mitosis (/10 high-power fields)	11.0±13.9	15.0±16.5	7.5±9.9	***<0.001***
Immunohistochemistry[d]				
EpCAM (positive)	89 (32.5)	55 (41.4)	31 (23.3)	***0.002***
K19 (positive)	34 (12.4)	26 (19.5)	7 (5.3)	***<0.001***
Ki-67 LI (%)	6.8 ± 9.5	7.8 ± 10.2	5.9 ± 8.8	0.110
Follow-up				
Recurrence[e]	153 (55.6)	83 (63.4)	67 (51.1)	
Deaths due to HCC	40 (14.5)	26 (19.4)	13 (9.8)	

[a] Values are presented as mean ± standard deviation or number (%).
[b] Size of largest tumor in case of multiple tumors
[c] Main or first order branches of portal vein and/or one or more of right, middle or left hepatic veins
[d] n=274
[e] Local recurrence or distant metastasisAFP, alpha-fetoprotein; HCC, hepatocellular carcinoma; NAFLD, non-alcoholic fatty liver disease; LI, labeling index

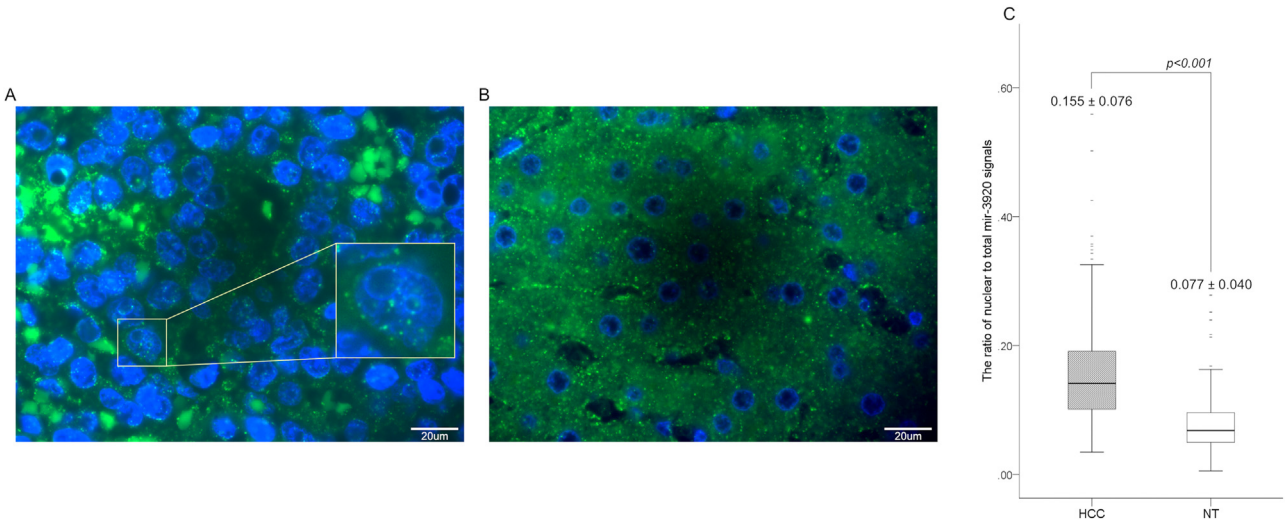

Fig. 1. LNA-FISH results demonstrating the expression of miR-3920 in HCC (boxed area shown at higher magnification in inset) (A) and non-neoplastic hepatocytes (B). The nuclear:total miR-3920 ratio was higher in HCC than in hepatocytes (C). (LNA-FISH, Locked nucleic acid fluorescence in situ hybridization; HCC, hepatocellular carcinomas; NT, non-neoplastic hepatocytes).

with stemness-related marker (EpCAM, K19) expression, aggressive clinicopathological features (e.g. microvascular invasion, major vessel invasion, and increased mitotic activity) and unfavorable prognosis.

MiR-3920, an 86-nucleotide miRNA located on the long arm of chromosome 11 (11q22.1), remains elusive in terms of its biological function or target genes. While a few studies have documented miR-3920 expression in tumors, its role in tumor development and progression remains uncertain. Hu et al. reported significant downregulation of miR-3920 in squamous cell carcinomas of the lung [17]. Conversely, Liu et al. identified miR-3920 as one of the significantly upregulated miRNAs in gastric car-

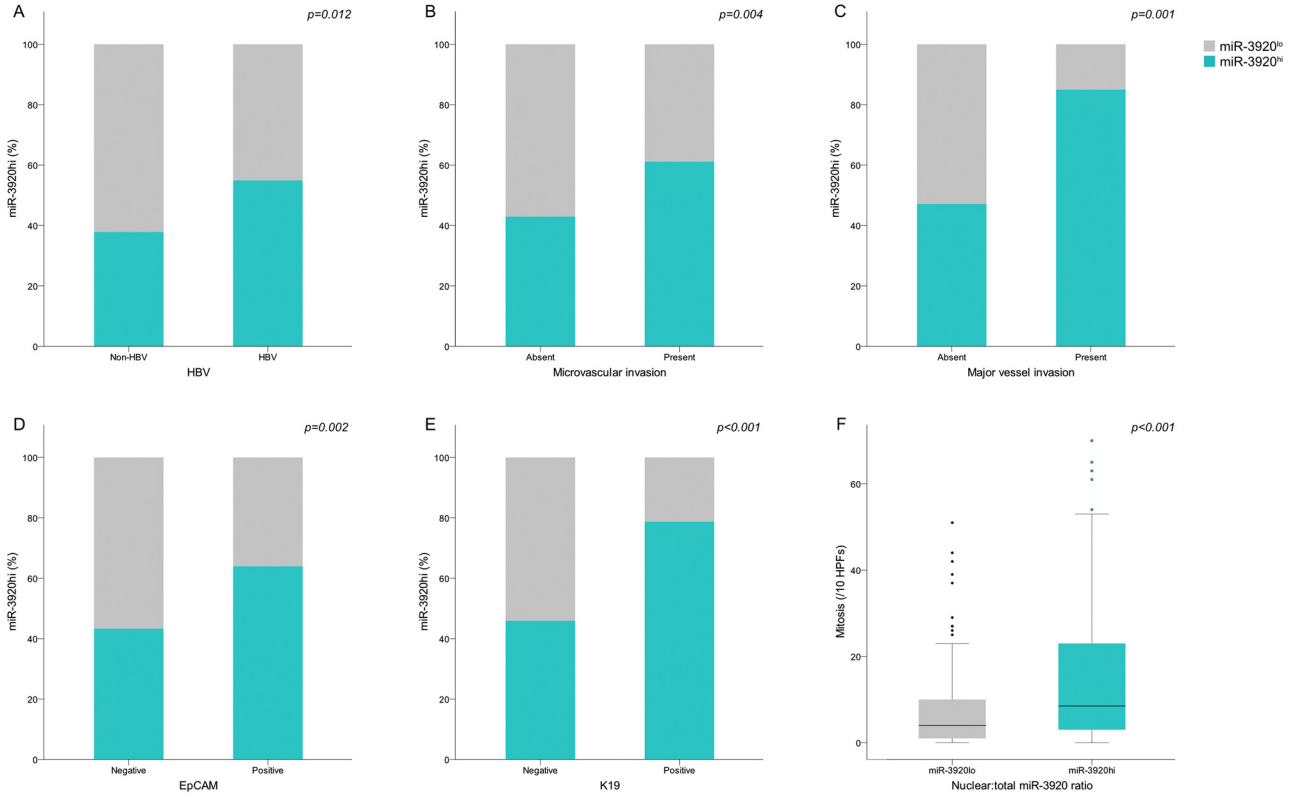

Fig. 2. Comparison of clinicopathological features between miR-3920^{hi} and miR-3920^{lo} hepatocellular carcinomas. MiR-3920^{hi} HCCs were more frequently associated with (A) hepatitis B viral etiology, (B) microvascular invasion, (C) major vascular invasion, (D) EpCAM and (E) K19 expression, and (F) higher mitotic indices.

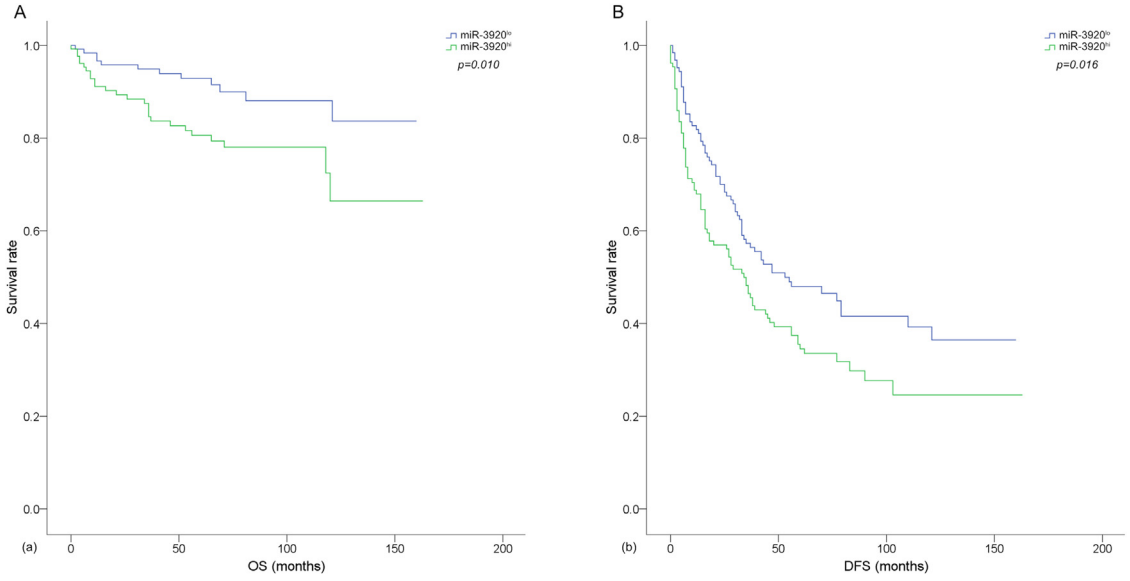

Fig. 3. Kaplan-Meier survival curves demonstrating decreased OS (A) and DFS (B) in miR-3920^{hi} and miR-3920^{lo} hepatocellular carcinomas. (OS, overall survival; DFS, disease-free survival).

cinoma [18]. Recent findings have suggested downregulation of miR-3920 as part of an m7G methylation-related miRNA signature that was predictive of poor prognosis in patients with endometrial cancer [19]. Abdolvand et al. identified miR-3920 as a miRNA that showed high binding scores with the long noncoding RNA KCNQ1OT1, which was increased in colorectal cancer tissues [20]. To our knowledge, the expression status of miR-3920 in HCCs and its clinicopathological implications have not yet been evaluated.

MiRNA maturation is controlled by nuclear and cytoplasmic regulation, and the maturation process predominantly occurs in the cytoplasm [21]. Although mature miRNAs were originally known to exist and function in the cytoplasm, more recent studies have demonstrated the existence of mature miRNAs in the nucleus. For example, miR-29b has been shown to contain a hexanucleotide element that facilitates nuclear import, resulting in its predominant localization within the nucleus [22]. Co-localization of mature miRNAs with Argonaute and TNRC6A proteins in the nucleus

Table 2
Survival analysis results.

Variable	Overall survival				Disease-free survival			
	Univariable analysis		Multivariable analysis		Univariable analysis		Multivariable analysis	
	HR (95% CI)	p-value	HR (95% CI)	p-value	HR (95% CI)	p-value	HR (95% CI)	p-value
Age (≥60)	0.733 (0.376-1.431)	0.363			0.869 (0.628-1.201)	0.394		
Sex (male)	1.349 (0.595-3.059)	0.473			1.403 (0.941-2.093)	0.097		
Etiology (HBV)	0.606 (0.267-1.376)	0.231			1.129 (0.784-1.625)	0.515		
Serum AFP (≥400 IU/mL)	1.342 (0.634-2.841)	0.443			1.067 (0.703-1.620)	0.761		
Tumor size (≥5 cm)	2.171 (1.113-4.235)	***0.023***	2.082 (1.058-4.098)	***0.034***	1.319 (0.904-1.925)	0.151		
Multiplicity	2.484 (1.255-4.915)	***0.009***	2.074 (1.021-4.213)	***0.044***	1.902 (1.302-2.777)	***0.001***	1.812 (1.234-2.661)	***0.002***
Edmondson-Steiner grade (III/IV)	0.919 (0.465-1.814)	0.807			1.033 (0.726-1.470)	0.857		
Microvascular invasion	1.872 (0.994-3.526)	0.052			1.380 (0.999-1.905)	0.051		
Major vessel invasion	2.937 (1.143-7.548)	***0.025***	2.134 (0.815-5.589)	0.114	1.413 (0.743-2.687)	0.292		
miR-3920^{hi}	2.381 (1.199-4.727)	***0.013***	2.318 (1.167-4.603)	***0.016***	1.479 (1.071-2.041)	***0.017***	1.439 (1.041-1.987)	***0.027***
EpCAM	1.705 (0.905-3.212)	0.099			0.963 (0.684-1.355)	0.827		
K19	1.852 (0.817-4.201)	0.140			1.308 (0.825-2.074)	0.253		
Mitosis (≥10/HPF)	1.621 (0.840-3.129)	0.150			0.966 (0.685-1.362)	0.844		
Ki-67 LI (≥30%)	0.588 (0.080-4.298)	0.601			0.977 (0.457-2.091)	0.952		

AFP, alpha-fetoprotein; CI, confidence interval; HBV, hepatitis B virus; HPF, high-power field; HR, hazard ratio; LI, labeling index

and cytoplasm has been demonstrated, in addition to cytoplasmic-to-nuclear transportation of these proteins via Importin 8 and Importin α/β, respectively [21,23]. The identification of mature nuclear miRNAs suggests the potential for miRNAs to act as gene regulators within this cellular compartment, beyond their classical role in post-transcriptional repression [21].

In contrast to the more commonly used methods such as real-time polymerase chain reaction for analysis of miRNA expression levels, in situ hybridization (ISH) techniques allow for a direct visualization of the subcellular localization of miRNAs. A few studies have demonstrated miRNAs that are predominantly located in the nuclei or nucleoli, suggesting that the subcellular localization of miRNAs may have functional implications [24–26]. For example, Li et al. identified 11 miRNAs with a nucleolar distribution in HeLa cells by ISH [25], and Khudayberdiev et al. demonstrated miRNAs with a nuclear distribution in dissociated hippocampal neurons using FISH methods [24]. Politz et al. used LNA in situ hybridization to demonstrate nucleolar miRNAs in rat myoblasts [26].

In our study, we used the LNA-ISH method on FFPE tissue sections in order to visually assess miRNA expression levels in specific cells (e.g., HCC tumor cell, non-neoplastic hepatocytes), in addition to the subcellular localization of the miRNA spots. The miRNA microarray analysis demonstrated higher miR-3920 expression in EpCAM-positive HCCs compared with EpCAM-negative HCCs. In contrast, the LNA-FISH analysis showed lower total miR-3920 signal counts in EpCAM-positive HCC cells. In addition, the total number of miR-3920 spots per cell were higher in the non-neoplastic hepatocytes than in the HCC tumor cells, contrary to our expectation. However, HCC is characterized by increased nuclear-to-cytoplasmic ratio compared to NT, resulting in a relatively smaller cytoplasmic area compared to non-neoplastic hepatocytes. Thus, we evaluated the nuclear miR-3920 signal counts and the nuclear/cytoplasmic ratio of miR-3920 signal counts per cell in our analysis. As a result, we found higher nuclear miR-3920 expression in HCCs compared with NT. Moreover, HCCs with higher nuclear miR-3920 expression were associated with stemness marker expression and aggressive behavior of HCC, such as higher proliferative activity (mitotic and Ki-67 labeling indices), and microvascular or major vascular invasion. Furthermore, OS and DFS were significantly lower for miR-3920^{hi} HCCs, and miR-3920 status was also an independent predictive factor of OS and DFS on multivariable analysis. Thus, the nuclear localization of miR-3920 might be linked to the aggressive behavior of HCC.

We were not able to find a functional relationship between miR-3920 expression and EpCAM expression in HCC cell lines, although there was a slight decrease in EpCAM expression levels after transfection with miR-3920 mimic. Thus, these findings are inconclusive for demonstrating a functional relationship between miR-3920 and EpCAM and do not establish a potential role for nuclear localization of miR-3920 in HCC stemness. However, it is an interesting possibility that transient ectopic expression of miR-3920 may not be sufficient to alter EpCAM expression in HCC cell lines, and that the nuclear localization of miR-3920 may play a more critical role in enhancing the stemness properties of HCC. Further in vitro analysis on stable transfected cell lines would be necessary to examine the potential functional relationship in more detail.

Another limitation of this study is that the majority of cases in our HCC cohorts were HBV-related. However, this reflects the regional characteristic of South Korea, where HBV is the predominant cause [27]. Our results would need to be validated in larger independent cohorts of HCC, including those where other etiologies are more predominant (i.e., non-HBV-related cohorts). Nevertheless, by using LNA-ISH, we demonstrate for the first time the clinicopatho-

logical significance of miR-3920 expression in HCCs, and also the importance of the subcellular localization of miR-3920 for predicting the behavior and prognosis of HCC.

Ethical statement

This study was approved by the Institutional Review Board of Seoul National University Bundang Hospital (B-2406-904-303).

Data sharing statement

The data analyzed in this study are included in the manuscripts and available from the corresponding author upon request.

Author contributions

Conceptualization: HK - Data curation: HP, HK, JEY - Formal analysis: HP, HL, SK - Funding acquisition: HK - Investigation: HP, HL, HK - Methodology: HP, HL, HN, SK - Project administration: HL, HK - Resources: HK, JEY - Software: HK, HP, SK - Supervision: HK, JEY - Validation: HK, JEY, HP, SK - Visualization: HP, SK - Writing - original draft: HP - Writing - review & editing: HP, HL, SK, HN, JEY, HK

Sources of funding

This study was supported by the National Research Foundation of Korea (NRF) grant funded by the Korea government (MSIT) (NRF-2013R1A1A2062320, 2019R1A2C2010056, 2022R1A2C2010348, RS-2025-23524841).

Declaration of competing interest

The authors have no conflicts of interests related to this publication. This statement applies to all listed authors.

Supplementary materials

Supplementary material associated with this article can be found, in the online version, at doi:10.1016/j.dld.2025.12.023.

References

[1] Huang DQ, Singal AG, Kanwal F, et al. Hepatocellular carcinoma surveillance — Utilization, barriers and the impact of changing aetiology. Nat Rev Gastroenterol Hepatol 2023;20:797–809.
[2] Siegel RL, Miller KD, Fuchs HE, et al. Cancer statistics, 2022. CA Cancer J Clin 2022;72:7–33.
[3] Sung H, Ferlay J, Siegel RL, et al. Global Cancer statistics 2020: GLOBOCAN estimates of incidence and mortality worldwide for 36 cancers in 185 countries. CA Cancer J Clin 2021;71:209–49.
[4] Renne SL, Di Tommaso L. A clinical and pathological update on hepatocellular carcinoma. J Liver Cancer 2022;22:14–22.
[5] Torbenson MS, Ng IOL, Park YN, et al. Hepatocellular carcinoma. In: WHO Classification of Tumours Editorial Board, editor. WHO Classification of Tumours of the Digestive System. Lyon: International Agency for Research on Cancer; 2019. p. 229–39.
[6] Rhee H, Kim HY, Choi JH, et al. Keratin 19 expression in hepatocellular carcinoma is regulated by fibroblast-derived HGF via a MET-ERK1/2-AP1 and SP1 axis. Cancer Res 2018;78:1619–31.
[7] Shu J, Silva B, Gao T, et al. Dynamic and modularized MicroRNA regulation and its implication in Human cancers. Sci Rep 2017;7:13356.
[8] Budhu A, Jia HL, Forgues M, et al. Identification of metastasis-related microRNAs in hepatocellular carcinoma. Hepatology 2008;47:897–907.
[9] Dang Y, Luo D, Rong M, et al. Underexpression of miR-34a in hepatocellular carcinoma and its contribution towards enhancement of proliferating inhibitory effects of agents targeting c-MET. PLoS One 2013;8:e61054.
[10] Huang YS, Dai Y, Yu XF, et al. Microarray analysis of microRNA expression in hepatocellular carcinoma and non-tumorous tissues without viral hepatitis. J Gastroenterol Hepatol 2008;23:87–94.
[11] Jiang J, Gusev Y, Aderca I, et al. Association of MicroRNA expression in hepatocellular carcinomas with hepatitis infection, cirrhosis, and patient survival. Clin Cancer Res 2008;14:419–27.
[12] Murakami Y, Yasuda T, Saigo K, et al. Comprehensive analysis of microRNA expression patterns in hepatocellular carcinoma and non-tumorous tissues. Oncogene 2006;25:2537–45.
[13] Guo J-C, Yang Y-J, Zhang J-Q, et al. microRNA-448 inhibits stemness maintenance and self-renewal of hepatocellular carcinoma stem cells through the MAGEA6-mediated AMPK signaling pathway. J Cell Physiol 2019;234:23461–74.
[14] Zhao B, Wang Y, Tan X, et al. Inflammatory micro-environment contributes to stemness properties and metastatic potential of HCC via the NF-κb/miR-497/SALL4 axis. Mol Ther- Oncolytics 2019;15:79–90.
[15] Tsai SC, Lin CC, Shih TC, et al. The miR-200b-ZEB1 circuit regulates diverse stemness of human hepatocellular carcinoma. Mol Carcinog 2017;56:2035–47.
[16] Li A, Yu J, Kim H, et al. MicroRNA array analysis finds elevated serum miR-1290 accurately distinguishes patients with low-stage pancreatic cancer from healthy and disease controls. Clin Cancer Res 2013;19:3600–10.
[17] Hu Y, Dingerdissen H, Gupta S, et al. Identification of key differentially expressed MicroRNAs in cancer patients through pan-cancer analysis. Comput Biol Med 2018;103:183–97.
[18] Liu D, Hu X, Zhou H, et al. Identification of aberrantly expressed miRNAs in gastric cancer. Gastroenterol Res Pr 2014;2014:473817.
[19] Chen R, Sun K, Hou Y, et al. Identification of m7G methylation-related miRNA signature associated with survival and immune microenvironment regulation in uterine corpus endometrial carcinoma. Biomed Res Int 2022;2022:8776678.
[20] Abdolvand M, Sadeghi M, Emami MH, et al. Constructing a novel competing endogenous RNAs network based on NR3C1 and X-linked inhibitor of apoptosis protein genes reveals potential prognostic biomarkers in colorectal cancer. J Res Med Sci 2022;27:71.
[21] Liu H, Lei C, He Q, et al. Nuclear functions of mammalian MicroRNAs in gene regulation, immunity and cancer. Mol Cancer 2018;17:64.
[22] Hwang H-W, Wentzel EA, Mendell JT. A hexanucleotide element directs MicroRNA nuclear import. Science 2007;315:97–100.
[23] Nishi K, Nishi A, Nagasawa T, et al. Human TNRC6A is an Argonaute-navigator protein for microRNA-mediated gene silencing in the nucleus. RNA 2013;19:17–35.
[24] Khudayberdiev SA, Zampa F, Rajman M, et al. A comprehensive characterization of the nuclear microRNA repertoire of post-mitotic neurons. Front Mol Neurosci 2013;6:43.
[25] Li ZF, Liang YM, Lau PN, et al. Dynamic localisation of mature microRNAs in Human nucleoli is influenced by exogenous genetic materials. PLoS One 2013;8:e70869.
[26] Politz JC, Hogan EM, Pederson T. MicroRNAs with a nucleolar location. RNA 2009;15:1705–15.
[27] Kim DY. Changing etiology and epidemiology of hepatocellular carcinoma: Asia and worldwide. J Liver Cancer 2024;24:62–70.